Achieving conductive high Al-content AlGaN alloys for deep UV photonics

Z.Y. Fan, J.Y. Lin and H.X. Jiang
Department of Physics, Kansas State University, Manhattan, Kansas 66506-2601, USA

ABSTRACT

Recent progresses in epitaxial growth and fundamental studies on electrical and optical properties of high Al-content AlGaN alloys with Si, Mg, and Zn doping are presented. For Si doped $Al_xGa_{1-x}N$, the Si activation energy was determined for x = 0 up to 1, and the resistivity of n-$Al_xGa_{1-x}N$ was found to increases by one order of magnitude when Al content is increased by ~ 8%. From photoluminescence (PL) studies, three groups of deep impurity transitions were observed, related with deep level acceptors involving cation vacancy and its complexes: $(V_{III})^{3-}$, $(V_{III}\text{-complex})^{2-}$, and $(V_{III}\text{-complex})^{1-}$, which are electron traps and compensating centers. By optimizing the growth processes to reduce the densities of cation vacancy and its complexes, the *n*-type conductivity of $Al_xGa_{1-x}N$ was significantly improved. A record low room temperature *n*-type resistivity of 0.0075 Ω·cm has been obtained for $Al_{0.7}Ga_{0.3}N$, and *n*-type conduction in pure AlN has also been achieved. We also review the electrical and optical measurement results of Mg-doped AlGaN and AlN. It was found that the overall material quality and conductivity of Mg-doped AlN are strongly correlated with the PL emission intensity of the nitrogen vacancy (V_N^{3+}) related transition. Improved conductivity was obtained by suppressing the V_N^{3+} related emission line, which was attributed to the reduced hole compensation by V_N^{3+}. With the identification of the emission peaks associated with V_N^{3+} hole compensating centers, the *p*-type conductivity of high Al-content AlGaN alloys was improved by monitoring and suppressing the intensity of the V_N^{3+} related emission lines. *P*-type conduction in $Al_xGa_{1-x}N$ (x > 0.7) was confirmed at elevated temperatures (> 700 K). The possibility of using Zn as an alternative *p*-type dopant was also studied. It was found that contrary to the calculation, the energy level of Zn acceptor in AlN was about 0.74 eV, which is 0.23 eV deeper than Mg level in AlN.

Keywords: III-nitride wide bandgap semiconductors, DUV photonics, *n*-AlGaN, *p*-AlGaN, conductivity, Si-doped AlGaN, Mg-doped AlGaN, Zn-doped AlN, activation energy.

1. INTRODUCTION

High-Al content AlGaN alloys, including pure AlN, are recognized as promising materials for applications in optoelectronic devices in deep ultraviolet (DUV) spectral range. Significant progresses are being achieved in AlGaN-based DUV LEDs[1], and 210 nm AlN-based PIN LED has been reported.[2] AlGaN based photodetectors are also being under intensively investigated.[3] Highly conductive, including *n*- and *p*-type high-Al content AlGaN alloys are essential for many DUV device applications.

With the huge strive to develop AlGaN-based compact UV LEDs, the efficiency and power output of these emitters are still very low. It has been found that the high Al content in AlGaN leads to a poor *p*- and *n*-type conductivity due to the deepening of the dopants levels and the compensation effect related with easily formed cation and anion vacancies, limiting the current injection and increasing the operation voltage. Different material structures have been proposed to improve the material quality and the UV LED power level, however, the attainment of highly conductive *p*-type AlGaN (of any Al composition) and *n*-type $Al_xGa_{1-x}N$ alloys (x > 0.7) remain one of the foremost challenging tasks of the Nitride community. Achieving highly conductive *n*-$Al_xGa_{1-x}N$ alloys with high Al contents is very difficult due to an increase in the ionization energy of the dopants and an enhanced compensation of native defects (cation vacancy and cation vacancy-complex) with an increase of the alloy composition,[4,5] while achieving *p*-type $Al_xGa_{1-x}N$ alloys with high Al-contents by Mg doping is much more challenging.

In this paper, we summarize some of the recent progresses made by our group at Kansas State University to achieve conductive *n*- and *p*-type AlGaN. Electrical and optical measurements were employed to study the Si, Mg and

Quantum Sensing and Nanophotonic Devices IV, edited by Manijeh Razeghi, Gail J. Brown,
Proc. of SPIE Vol. 6479, 64791I, (2007) · 0277-786X/07/$18 · doi: 10.1117/12.715046

Zn doped AlGaN alloys with high Al content up to pure AlN, with the aim to explore the fundamental reasons limiting the *n*- and *p*-type conductivity in AlGaN, and the possible approaches to overcome these difficulties.

2. EXPERIMENT

$Al_xGa_{1-x}N$ and AlN epilayers with about 1 μm thick were grown on AlN/sapphire (0001) substrates by metal organic chemical vapor deposition (MOCVD). High quality, undoped AlN epilayer template plays an important role to reduce dislocations in the subsequent doped layer. The metal organic sources used were trimethylgallium (TMGa) for Ga and trimethylaluminum (TMAl) for Al, and blue ammonia (NH_3) was the gas source for N. Silane (SiH_4), bis-cyclopentadienyl-magnesium (Cp_2Mg), and dimethyl zinc (DMZn) were used for Si, Mg, and Zn doping, respectively. The doping level was varied by controlling their flow rates. The Al contents of AlGaN alloys were determined by energy dispersive x-ray (EDX) and x-ray diffraction (XRD) measurements as well as by the flow rates of TMGa and TMAl. The Al contents determined by all three methods agreed within ±0.02. Secondary ion mass spectroscopy (SIMS) measurements were also performed (by Charles Evan & Associates) for selective samples to verify the Si and Mg dopant concentrations. Atomic force microscopy (AFM) and scanning electron microscopy (SEM) were employed to examine the surfaces and revealed crack-free epilayers. Variable temperature (up to 900 ^oC) Hall-effect (standard Van der Pauw) measurements were used to measure the electron concentration, mobility, and resistivity of these materials. A deep UV (5 mW @ 197 nm) picosecond time-resolved photoluminescence (PL) spectroscopy system was specially designed to probe the optical properties of materials and device structures based on AlGaN alloys with high Al contents. The deep UV PL system consists of a frequency quadrupled 100 femtosecond Ti:sapphire laser with an excitation photon energy around 6.28 eV (with a 76 MHz repetition rate), a monochromator (1.3 m), and a streak camera with a detection capability ranging from 185 – 800 nm and a time resolution of 2 ps.

3. RESULTS AND DISCUSSIONS

3.1 Si dopants activation energy in *n*-AlGaN[6]

One of the difficulties to achieve highly conductive $Al_xGa_{1-x}N$ alloys with high Al contents is caused by the increase of the ionization energy of the dopants with increasing Al content. In this section, we report the determination of Si dopants activation energy in $Al_xGa_{1-x}N$ alloy with x from 0 to 1. The electrical transport properties of Si-doped *n*-type $Al_xGa_{1-x}N$ epilayers with Si dopant concentration (N_{Si}) of 3.5×10^{19} cm^{-3} in all samples were studied. From the room temperature Hall measurement results, we found that the resistivity of *n*-$Al_xGa_{1-x}N$ increases by one order of magnitude when Al content is increased by ~ 8%. This rapid increase in resistivity is predominantly due to an increase in donor ionization energy, which is demonstrated by the activation (ionization) energy dependence on Al content, shown in Fig. 1. Here the resistivity at different temperature was measured, and the activation energy E_0 is obtained by fitting the temperature dependent resistivity data with equation

$$\rho = \rho_0 / \left[1 + C \exp\left(-E_0 / kT\right)\right] \qquad (1)$$

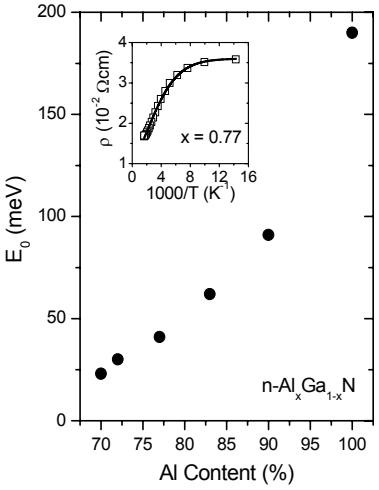

Fig. 1. Si donor activation energy as a function of the Al content, x [After Ref. 6]

where C is a fitting constant and k is the Boltzmann constant, illustrated in the inset of Fig. 1. From Fig. 1, E_0 increases with an increase of the Al content. This deepening of E_0 is due to the fact that with an increase of the Al content in AlGaN alloys, the bandgap and electron effective mass increase, while the dielectric constant and band gap renormalization effect decrease. For pure AlN, an estimated value of E_0 of about 190 meV is obtained for our AlN sample. Taniyasu et al estimated the donor ionization energy in AlN of about 86 meV.[7] Our experimental results indicate that we have achieved measurable

conductivity in pure AlN. We believe that the predominant cause for the rapid increase in resistivity of $Al_xGa_{1-x}N$ alloys with high Al contents is the Si donor level deepening, a direct consequence of Eq. (1), which can be approximately written as $\rho \propto exp(E_0/kT)$ at a fixed temperature when $E_0 > kT$. Thus, the resistivity of $Al_xGa_{1-x}N$ alloys with high Al contents increases exponentially with the Si donor activation energy.

3.2 Deep impurity traps influencing *n*-AlGaN conductivity[8,9]

Here we summarize the investigations of deep impurity transitions in $Al_xGa_{1-x}N$ epilayers with x up to 1 to identify the properties of these transitions and their influence on the *n*-type conductivity of $Al_xGa_{1-x}N$ epilayers. Theoretical calculations have indicated that the cation vacancy and its complex in undoped and Si-doped AlGaN alloys, particularly in Al-rich alloys have small formation energies and are easily formed during crystal growth.[10,11] Three groups of transitions involving deep level impurities have been identified. In Fig. 2, we plot the room temperature PL spectral peak position (E_{imp}) of these three groups of impurity transitions in $Al_xGa_{1-x}N$ alloys as functions of x. The energy positions of the three different impurity transitions show a continuous increase with x and follow the same trend, indicating that they are of the similar nature.

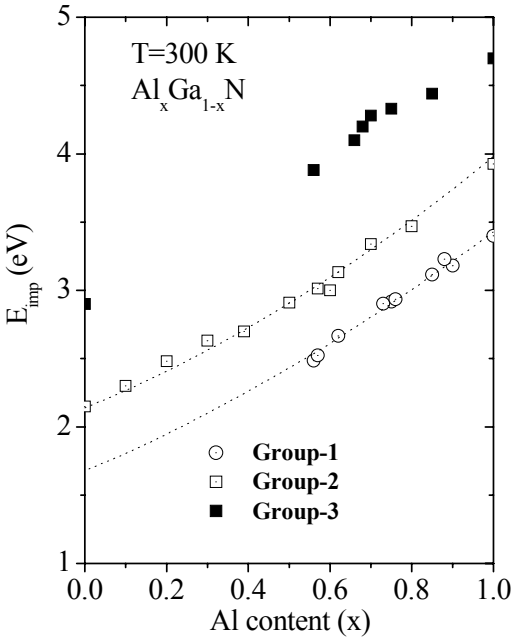

Fig. 2. PL peak position of the three groups of observed impurity transitions in $Al_xGa_{1-x}N$ as function of Al content x. Dotted lines are guide to the eyes [After Ref. 9].

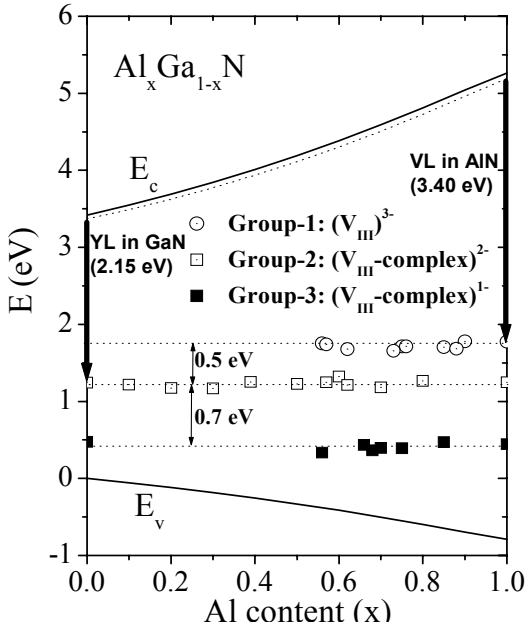

Fig. 3. The deep acceptor energy levels associated with $(V_{III})^{3-}$, $(V_{III}\text{-complex})^{2-}$, and $(V_{III}\text{-complex})^{1-}$, plotted as a function of the Al content, x [After Ref. 9].

The peak energies of deep level impurity transitions in group 1 were measured from a set of samples with relatively low impurity concentrations. Starting from the yellow line (YL) around 2.15 eV in GaN, the peak energy of this group of deep impurity transition blue shifts with increasing Al concentration to 3.90 eV for AlN. Another group of deep impurity transition (group 2), which is distinctly different from the YL in GaN, was observed in a set of $Al_xGa_{1-x}N$ epilayers with higher impurity concentrations due to doping with Si or unintentional doping with O, and this group of transition only happens for $x > 0.58$, and the violet line (VL) in AlN at 3.40 eV belongs to this group. By reducing the above two different deep impurity transitions through growth optimization, Al-rich $Al_xGa_{1-x}N$ alloys show improved conductivity, and a new group of deep impurity transition was observed in the optimized $Al_xGa_{1-x}N$ epilayers, shown in Fig. 2 as group 3. The spectral peak positions of this group of deep impurity transitions blue shift from 2.86 eV in GaN to 4.71 eV in AlN.

To identify the origins of these deep impurity transitions, we plot the deep acceptor energy levels (E_A) with E_v and E_c as functions of x in Fig. 3. In obtaining Fig. 3, we used the commonly known compositional dependence of the bangap of $Al_xGa_{1-x}N$,

$$E_g(x) = (1-x)E_g(GaN) + xE_g(AlN) - bx(1-x) \quad (2)$$

where the bowing parameter b and the room temperature energy bandgaps of GaN and AlN were taken as 1, 3.44 and 6.05 eV, respectively.[12] The conduction (E_c) and valence (E_v) band offset parameters have been assumed to be 70% and 30% for $Al_xGa_{1-x}N$ ($0 \le x \le 1$) alloys, respectively. The valence band maximum of GaN was chosen as E=0. The three groups of deep impurity transitions are attributed to donor-to-acceptor pair (DAP) transitions between a shallow donor and three different acceptor levels. PL lifetime measurements show these transitions have very long decay lifetime (> 1 μs), supporting this assumption. The chemical origin of the shallow donors involved here is believed to be either Si or O in $Al_xGa_{1-x}N$ alloys. Assuming the ionization energies of the shallow donors (E_D^0) increase linearly from 25 to 86 meV with varying x from 0 to 1 in $Al_xGa_{1-x}N$ alloys[7], the acceptor level (E_A) deduced from Figs. 2 with neglecting the Coulomb interaction between the ionized donors and acceptors is then given by,

$$E_A = E_g(x) - E_{imp} - E_D + E_v \quad (3)$$

where $E_v = -0.3\Delta E_g(x)$ and $E_c = E_g(GaN) + 0.7\,\Delta E_g(x)$. E_A is plotted in Fig. 3 together with E_c and E_v as functions of x. It is interesting to note that the deduced acceptor levels as functions of x are horizontal lines in the whole range of x. This clearly indicates that these levels are pinned to the energy levels common to $Al_xGa_{1-x}N$ alloys with an energy separation of 0.5 eV between group 1 and group 2, and 0.7 eV between group 2 and group 3. This is very common for deep acceptors in other semiconductors as well as in III-nitrides as a consequence of the large binding energies and very strong localization of deep acceptors. [13]

The formation energies (E_{form}) of V_{III} and V_{III} complexes as well as other impurities as functions of Fermi level, E_F, have been calculated in GaN and AlN.[14,10,11] Since $(V_{Ga}\text{-complex})^{2-}$ has the lowest E_{form} regardless of E_F in GaN, the origin of the YL in GaN is attributed to $(V_{Ga}\text{-complex})^{2-}$ such as V_{Ga}–O_N or V_{Ga}–Si_{Ga} rather than isolated $(V_{Ga})^{2-}$ or $(V_{Ga})^{3-}$. The energy peaks in this group (Group-1) are thus attributed to the transition between a shallow donor level to a deep acceptor level $(V_{III}\text{-complex})^{2-}$. However, the E_{form} of $(V_{III})^{3-}$ decreases with increasing x in $Al_xGa_{1-x}N$ alloys and becomes the lowest and negative with increasing E_F (E_F>5.8 eV) in AlN, indicating that $(V_{III})^{3-}$ can be formed spontaneously during the growth of AlN. Thus, $(V_{III})^{3-}$ is the most favorable native defect and accountable for the VL (3.40 eV) in AlN with high impurity concentrations, in which E_F is relatively high. So the commonly observed VL in AlN is a DAP transition involving a shallow donor and a $(V_{Al})^{3-}$ deep acceptor, and the energy peaks in this group (Group-2) are thus attributed to the transition between a shallow donor level to a deep acceptor level $(V_{III})^{3-}$. The possibility of $(V_{Al})^{2-}$ as the origin of a deep acceptor in $Al_xGa_{1-x}N$ alloys can be excluded due to its higher formation energy than $(V_{Al}\text{-complex})^{2-}$. The binding energies of $(V_{Al})^{3-}$ and $(V_{Al}\text{-complex})^{2-}$ in AlN can be obtained from Fig. 3 to be about 2.60 and 2.10 eV (with a difference of 0.50 eV), respectively. The calculated binding energy of $(V_{Al})^{3-}$ varies from 2.10 to 2.60 eV, while that of $(V_{Al}\text{-complex})^{2-}$ is about 1.60–1.90 eV. The calculated difference in binding energies between $(V_{Al})^{3-}$ and $(V_{Al}\text{-complex})^{2-}$ is about 0.5 eV, which agrees very well with our experimental value. These facts again support our assignment that acceptors involved in the DAP transitions in group 1 and 2 are $(V_{III}\text{-complex})^{2-}$ and $(V_{III})^{3-}$, repectively. The absence of deep impurity transitions related with $(V_{III})^{3-}$ for materials with x<0.58 is consistent with the fact that $(V_{III}\text{-complex})^{2-}$ are more favorable in $Al_xGa_{1-x}N$ alloys with low x (x<0.58). The existence of strong deep impurity transitions related with $(V_{III})^{3-}$ also correlates with reduced electrical conductivities in $Al_xGa_{1-x}N$ alloys with x>0.58. Our experimental results support the claim that $(V_{III})^{3-}$ is very stable, giving the strong deep impurity transitions in $Al_xGa_{1-x}N$ alloys with x>0.58, which may be a cause of the reduced *n*-type conductivity in $Al_xGa_{1-x}N$ alloys with high x, particularly in AlN, due to its ability to capture three electrons.

The calculation also shows that the formation energies of $(V_{III})^{3-}$ and $(V_{III}\text{-complex})^{2-}$ are lower than that of $(V_{III}\text{-complex})^{1-}$ and anion vacancies cannot be formed in Si doped GaN and AlN. From the energy position relative to the those of $(V_{III})^{3-}$ and $(V_{III}\text{-complex})^{2-}$, we believe that the deep level acceptor involved in the Group-3 impurity transitions is cation vacancy complex with one-negative charge $(V_{III}\text{-complex})^{1-}$, such as $(V_{Ga}\text{-}2O_N)^{1-}$. The possibility of isolated $(V_{III})^{1-}$ as the origin of the newly observed deep acceptor in $Al_xGa_{1-x}N$ alloys can be excluded due to its much higher formation energy than $(V_{III}\text{-complex})^{1-}$. The binding energies of the $(V_{III}\text{-}2O_N)^{1-}$ deep level acceptors increase almost linearly from about 0.55 to 1.25 eV with varying x from 0 to 1 in $Al_xGa_{1-x}N$ alloys. The calculated binding energy of $(V_{Al}\text{-}2O_N)^{1-}$ ranges from 1.0 to 1.12 eV in AlN. The calculated differences in binding energies between $(V_{III})^{3-}$

and $(V_{Al}\text{-}O_N)^{2-}$ and between $(V_{Al}\text{-}O_N)^{2-}$ and $(V_{Al}\text{-}2O_N)^{1-}$ in AlN, respectively, are about 0.5 and 0.7 eV, which agree perfectly with our experimentally measured values shown in Fig. 3 (0.5 and 0.7 eV).

In summary, we have investigated the impurity transitions in $Al_xGa_{1-x}N$ epilayers between x=0 and 1. Three groups of deep impurity transitions were observed. The origins of three different acceptors involved in the deep impurity transitions have been identified as $(V_{III}\text{-complex})^{2-}$ in $Al_xGa_{1-x}N$ alloys between x=0 and 1 and $(V_{III})^{3-}$ in $Al_xGa_{1-x}N$ alloys between x=0.58 and 1, and the third one $(V_{III}\text{-complex})^{1-}$ in $Al_xGa_{1-x}N$ alloys between x=0 and 1 with improved conductivity. The YL and VL in GaN and AlN have been identified as different special cases of these impurity transitions in AlGaN alloys. Our experimental results indicate that the formation of $(V_{III})^{3-}$ is more favorable in Al-rich AlGaN alloys, while $(V_{III}\text{-complex})^{2-}$ are more favorable in $Al_xGa_{1-x}N$ alloys with lower x. The three acceptor levels are pinned to the energy levels common to $Al_xGa_{1-x}N$ alloys with an energy separation of 0.5 eV between $(V_{III})^{3-}$ and $(V_{III}\text{-complex})^{2-}$, and 0.7 eV between $(V_{III}\text{-complex})^{2-}$ and $(V_{III}\text{-complex})^{1-}$. The presence of these deep acceptor levels trap electrons, leading to the reduced conductivities of *n*-$Al_xGa_{1-x}N$.

3.3 Achieving highly conductive *n*-AlGaN[9]

As have been demonstrated, achieving highly conductive $Al_xGa_{1-x}N$ alloys with high Al contents is found to be very challenging due to (i) an increase in the ionization energy of the Si dopants with increasing Al content, and (ii) deep level transitions caused by cation vacancies (and complex) with triple, double and single negative charges by trapping electrons, and the formation energy of the triple-charged vacancies decreases with increasing Al content and becomes very low in AlN. Although the ionization energy of Si dopants cannot be changed, reduction of electron traps by optimizing the growth to diminish the cation vacancies (and complex) can be achieved.

Since $(V_{III}\text{-}2O_N)^{1-}$ captures only one electron, their presence will not detriment the conductivity as severely as the presence of $(V_{III})^{3-}$ and $(V_{Al}\text{-}O_N)^{2-}$ defects, which is consistent with our experimental results presented in Fig. 4. Fig. 4 illustrates the evolution of room temperature (300 K) PL spectra and resistivity of $Al_xGa_{1-x}N$ alloys (x~0.66) grown under various conditions. The arrows indicate the spectral peak positions of the spectra. All samples exhibit a bandedge transition at 5.10 eV and the bandedge emission intensity increases with decreasing resistivity. As shown in Fig. 4(a), for an early grown Si-doped $Al_{0.66}Ga_{0.34}N$ alloy with high resistivity (beyond our instrument limitation), the dominant impurity peak at 2.84 eV is related to the isolated cation vacancy, $(V_{III})^{3-}$. The triply charged cation vacancy captures three electrons and thus their presence significantly increases the resistivity. As illustrated in Fig. 4(b), suppression of $(V_{III})^{3-}$ related transition results in a reduction in resistivity to 1.8 Ωcm and simultaneously an emission peak at 3.31 associated with the presence of $(V_{III}\text{-complex})^{2-}$. Since V_{III}^{3-} and $(V_{III}\text{-complex})^{2-}$ defects in AlGaN alloys capture three and two electrons, respectively, these defects act as compensating centers for *n*-type doping and their densities have to be minimized in order to further enhance the conductivity. As illustrated in Fig. 4(c), once $(V_{III})^{3-}$ and $(V_{III}\text{-complex})^{2-}$ related transitions were suppressed by varying the growth conditions, we have significantly reduced the sample resistivity to 0.026 Ωcm. However, the newly identified impurity transition involving $(V_{III}\text{-complex})^{1-}$ at 4.10 eV is evident. We believe that the conductivities of Al-rich AlGaN alloys and pure AlN will continue to improve by further reducing the densities of the intrinsic defects - cation vacancies (and complexes) with triple, double, and single negative charges.

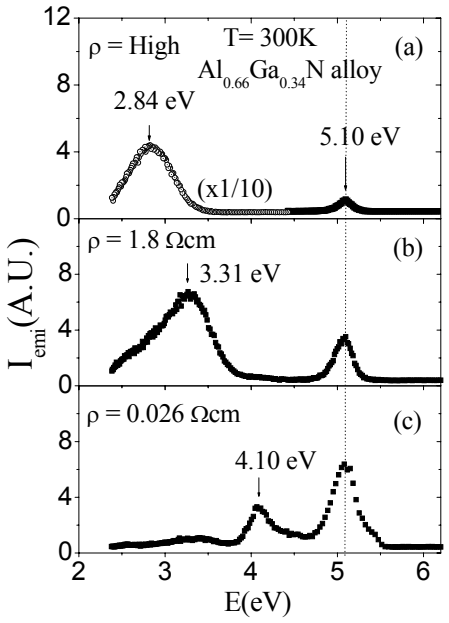

Fig. 4. Si donor activation energy as a function of the Al content, x [After Ref. 9].

With the optimized growth condition to reduce the cation vacancy and the reduction of oxygen concentration in our epilayers, a record low room temperature *n*-type resistivity for Al-rich AlGaN alloys have been achieved, specifically, a resistivity of 0.0075 Ω·cm (with an electron concentration of 3.3×10^{19} cm^{-3} and mobility of 25 cm^2/Vs) has been obtained for $Al_{0.7}Ga_{0.3}N$. Transport measurement indicates that we have also achieved *n*-type conduction in pure AlN.

3.4 Mg dopants activation energy in *p*-AlGaN[15]

Contrasting with the impressive results of conductive *n*-AlGaN, achieving *p*-AlGaN with high Al content is more challenging due to the large activation energy of the Mg acceptor. For the development of high performance DUV emitters and detectors with $\lambda < 280$ nm, it is imperative to investigate the limitation and methods of *p*-type doping in Al-rich AlGaN alloys and pure AlN. In the following sections, we review the electrical and optical measurement results of Mg-doped AlGaN and AlN, determining the activation energy of Mg dopants in AlGaN, elucidating the impurities limiting the hole generation, addressing the physical mechanisms limiting the *p*-type conductivity. The possibility of using Zn as an alternative *p*-type dopant is also studied.

We investigated Mg-doped $Al_xGa_{1-x}N$ and AlN epilayers by employing deep UV picosecond time-resolved PL spectroscopy to study the optical transitions. From PL emission spectra and the temperature dependence of the PL emission intensity, the Mg acceptor activation energy in $Al_xGa_{1-x}N$ as a function of the Al content (x) was extrapolated for the entire AlN composition range. At room temperature, PL emission lines due to band-to-impurity transitions of free electrons with neutral Mg acceptors in $Al_xGa_{1-x}N$ alloys with low x value have been observed, from which the values of the Mg acceptor activation energy E_A were deduced, which are consistent with the Hall measurement results.[16] The determination of Mg energy level in AlN is more complex. Comparing the PL spectra of Mg-doped and undoped AlN, we found that Mg-doped AlN exhibits two dominant emission lines at 4.70 and 5.54 eV at low temperature of 10K, which are absent in undoped AlN and are thus attributed to Mg impurity related transitions. The spectral peak positions of these emission lines suggest that they are either band-to-impurity or DAP transitions. However, the slow component of the recombination lifetimes of both emission lines measured at 10 K are about 1 μs, which precludes the possibility for the band-to-impurity type transitions which are known to have a recombination lifetime in the order of 1 ns. By fitting the PL intensity of the 5.54 eV emission line at different temperature with equation

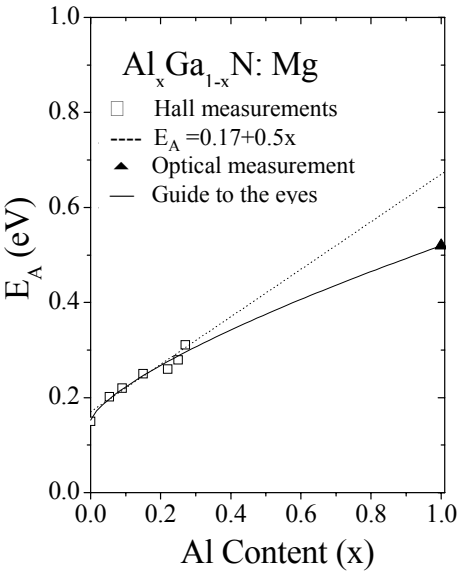

Fig. 5. Mg acceptor activation energy in Mg-doped $Al_xGa_{1-x}N$ as a function of the Al content (x). Open squares are data from Hall effect measurements, while the filled triangle is the data for AlN from PL measurements. The dotted line is the linear extrapolation of data from Hall results and the solid line is a guide to the eyes [After Ref.15].

$$I_{emi}(T) = I_0 / \left[1 + C \exp\left(-E_0 / kT\right)\right] \qquad (4)$$

where E_0 is the activation energy of the PL emission intensity, we found an activation energy of 0.06 eV for the 5.54 eV emission line, suggesting this emission line is a DAP transition between the Mg acceptor and a shallow donor (with an ionization energy of 0.06 eV). By neglecting the Coulomb interaction between the ionized donors and acceptors, a value of E_A=0.52 eV for the Mg acceptor binding energy in AlN is deduced from $E_A \approx E_g$-5.54 eV-0.06 eV with E_g=6.12 eV at 10 K. Similarly, we attribute the 4.70 eV emission line to be the transition between a deep level donor (E_D = 0.90 eV) and the Mg acceptor level of about 0.51 eV above the valence band of AlN. By this method, we determined Mg energy level in AlN is 0.51 eV (±0.01), which is close to the lower limit values obtained by the effective mass theory.

Fig. 5 presents the determined Mg acceptor ionization energy in $Al_xGa_{1x}N$ and AlN as a function of the Al content x. The dotted line is the linear extrapolation of data from $Al_xGa_{1-x}N$ alloy with low Al content. The solid line is guide to the eyes by including the value in Mg-doped AlN. It is clear that the activation energy increases with the bandgap, as predicted by the effective mass theory.

3.5 Deep impurity transitions influencing *p*-AlGaN conductivity [17]

As we have discusses in section 3.2, compensation by native defects such as $(V_{III})^{3-}$, $(V_{III}\text{-complex})^{2-}$, and $(V_{III}\text{-complex})^{1-}$ limits the *n*-type conductivity of AlGaN. In Mg doped AlGaN alloys, nitrogen vacancies play a similar role in limiting *p*-type conductivity of AlGaN. The study of correlation between optical and electrical properties of Mg-doped AlN elucidates the related impurities.

Figure 6 compares the room temperature (300 K) PL spectra of (a) an undoped AlN epilayer, (b) a Mg-doped AlN epilayer with high resistivity, and (c) a Mg-doped AlN epilayer with improved *p*-type conductivity (or reduced resistivity). The arrows indicate the spectral peak positions. Undoped AlN has a strong band-edge emission peak at 5.98 eV due to the recombination of free excitons and exhibits virtually no impurity transitions in the low energy region, ensuring a good optical quality. AFM revealed an atomically smooth surface with a root mean square (rms) roughness of about 7 Å within a 2 μm x 2 μm scan. These undoped AlN epilayers were employed as templates for the subsequent growth of Mg-doped AlN epilayers. For Mg-doped AlN epilayers, the PL spectra presented in Figs. 6(b) and 6(c) encompass an emission peak at around 4.7 eV, in addition to the band-edge emission at 5.94 eV. The band-edge emission peak at 5.94 eV is due to the recombination of excitons bound to neutral Mg acceptors (or acceptor-bound excitons I_1). The energy separation between the I_1 and free exciton transitions is 40 meV, corresponding to the binding energy, E_{bx}, of the acceptor-bound exciton (I_1).

A clear correlation between the electrical and optical properties of Mg-doped AlN epilayers has been observed. Samples exhibiting strong emissions at 4.7 eV, such as that shown in Fig. 6(b), are generally highly insulating. By varying the growth conditions, especially the V/III ratio, the intensity of the impurity emission peak at 4.7 eV was significantly suppressed, the I_1 transition at 5.94 eV was enhanced, and the conductivity was improved. It is also interesting to note that the I_1 transition in Mg-doped AlN epilayers survives well up to room temperature due to its large binding energy of 40 meV. In general, bound exciton transitions are not observable in Mg-doped GaN at room temperature. For the Mg-doped AlN epilayer with improved conductivity (Fig. 6(c)), additional emission peaks at 5.36 and 5.55 eV, which were absent in highly resistive Mg-doped samples, are evident.

The Mg concentration profile in the Mg-doped AlN epilayer has been probed by SIMS with a Mg-concentration on the order of 10^{20} cm^{-3}. Hall-effect measurements were carried out at elevated temperatures. The resistivity for one of our Mg-doped AlN epilayers, in which the intensity of the 4.7 eV emission line was minimized, was measured in the temperature range between 400 and 900 K and the result is shown in Fig 7. In order to verify that the conduction at high temperatures is due to hole activation from Mg acceptors, we have obtained the thermal activation energy of the resistivity by fitting the measured temperature dependent resistivity by the relation

$$\rho(T) = \rho_o e^{E_A/KT} \qquad (5)$$

where ρ(T) is the resistivity at temperature T. The fitted value of E_A is about 0.40 eV. Assuming a temperature dependent mobility of $\mu \propto T^{-3/2}$ at high temperatures, the fitted E_A value becomes 0.5 eV. This value agrees perfectly with the Mg acceptor energy level obtained from previous optical measurements shown in Fig. 5. Thus, the measurable conductivity at high temperatures is due to the conduction of holes.

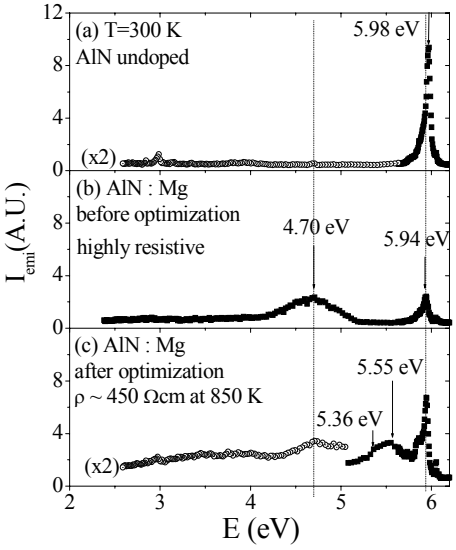

Fig. 6. Room temperature PL spectra of (a) an undoped and highly resistive AlN epilayer, (b) Mg-doped and high resistive AlN epilayer and (c) Mg-doped AlN epilayer with improved conductivity [After Ref.17].

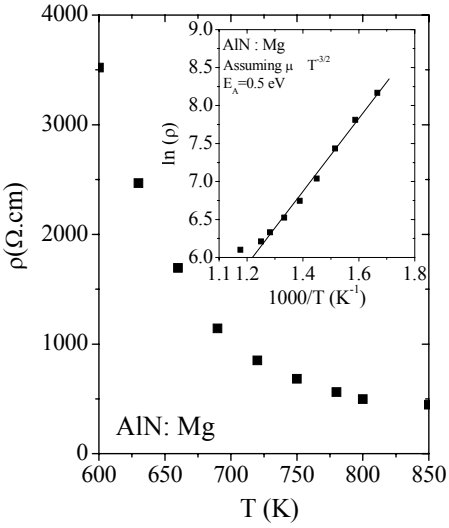

Fig. 7. Temperature variation of resistivity of the Mg-doped AlN epilayer in the temperature range of 400 - 900 K. Inset is the Arrhenius plot of ρ vs T. The solid line is the least square fit of data with Eq. (5). The fitted value of E_A, is 320 meV (396 meV) without (with) considering the variation of μ with T ($\mu \propto T^{-3/2}$). [After Ref. 17].

The intensity of the 4.7 eV emission line was carefully monitored while the growth conditions were varied. A general trend is that a strong emission peak at 4.7 eV translates to a highly resistive material even after thermal annealing. The *p*-type conductivity enhances with decreasing the emission intensity of the 4.7 eV line. This correlation clearly indicates that the 4.7 eV emission line is related with hole compensating centers. Theoretical calculations have indicated that nitrogen vacancies (V_N) have small formation energy in Mg-doped AlN, which further decreases when the Fermi energy level moves toward the valence band.[10] The formation energy of nitrogen vacancies with three positive charges (V_N^{3+}) is smaller than that with one positive charge (V_N^{1+}). Thus the generation of V_N^{3+} is more favorable during the growth of Mg-doped AlN. V_N^{3+} deep donors can compensate free holes in acceptor-doped materials. Once the density of V_N^{3+} deep donors is minimized by varying the growth conditions, the emission intensity of the 4.7 eV line is reduced, and concomitantly, the conductivity is enhanced. In samples with improved conductivity, more neutral Mg impurities are also available. This is also evident from the increased emission intensity of the free electron to neutral Mg (Mg^o) transition at 5.55 eV, and the I_1 transition at 5.94 eV. We assign the emission peak at 5.55 eV to the free electrons to Mg^o transition because the spectral peak position is consistent with the measured Mg energy level and bandgap of AlN (6.06 eV- 0.50 eV = 5.56 eV). Due to its strong correlation with the conductivity, we attribute the emission peak at 4.7 eV to the donor and acceptor pair (DAP) recombination involving electrons bound to V_N^{3+} deep donors and Mg^o in Mg-doped AlN. The enhanced conductivity is due to the suppressed compensating native defects (V_N^{3+}) in the optimized samples. Thus, we believe that monitoring the V_N^{3+} related PL emission provides an effective way for AlN material and p-type conductivity optimization.

Based on our experimental results, we have constructed an energy level diagram involving Mg acceptors and hole compensating centers in Mg-doped AlN in Fig. 8. We have taken the bandgap of AlN to be 6.06 eV at room temperature and free exciton binding energy to be 80 meV.[18] The magnesium level is 0.50 eV above the valence band. Coulomb interaction term between the ionized donors and acceptors has been neglected in the calculations. From the emission line at 4.7 eV, the energy level of V_N^{3+} can be calculated as $E_D \approx E_g - 4.7$ eV- 0.50 eV $\approx$ 0.86 eV. Theoretically calculated energy level of V_N^{3+} is about 0.9 eV,[19] which is close to our measured value. We have previously observed a nitrogen vacancy (V_N) related transition in ion-implanted AlN epilayers and determined a binding energy of about 0.26 eV.[20] Since this value is smaller than the binding energy of V_N^{3+} observed here, we believe the nitrogen vacancies in ion-implanted AlN are singly charged state (V_N^{1+}). By including this level in the energy diagram, a possible transition involving V_N^{1+} and Mg^o would give rise to an emission peak at about 5.29 eV. The emission line observed at about 5.36 eV in Fig. 6(c) is close to the spectral peak position of this proposed transition by noticing that the Coulomb interaction term between the donor and acceptor has been neglected.

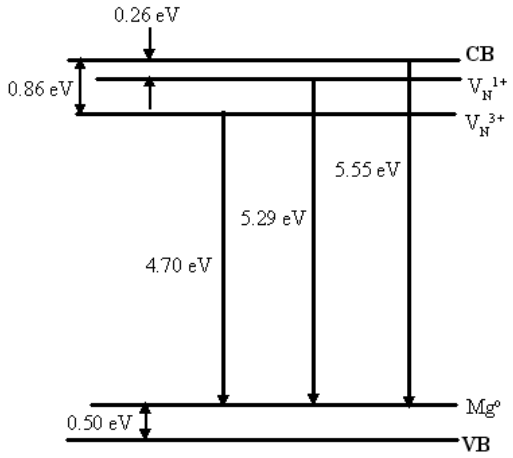

Fig. 8. Energy level diagram of nitrogen vacancies and Mg acceptors in Mg-doped AlN. [After Ref.17].

In summary, a strong correlation between the optical and electrical properties was observed in Mg-doped AlN. For highly resistive samples, a strong emission peak at 4.7 eV associated with the transition of electrons bound to V_N^{3+} to neutral Mg was observed. Enhanced conductivities were obtained in samples that exhibit a suppressed PL emission peak at 4.7 eV and enhanced acceptor-bound-exciton emission peak at 5.94 eV. The enhanced *p*-type conductivity is attributed to the reduced hole compensation by the donor-like intrinsic defects mainly related with V_N^{3+}. From the temperature dependent Hall-effect measurement, a value of 0.5 eV for the Mg acceptor activation energy in AlN has been obtained, which agrees with the value obtained by previous optical measurements.

3.6 Zn-doped AlN[21]

Since the activation energy of Mg is about 0.51 eV in AlN, it is very difficult to achieve a reasonable *p*-type conductivity in AlN and Al-rich AlGaN. Exploring alternative dopants seems to be inevitable. Zn element has been previously utilized as *p*-type dopants in GaN, which, however, rendered semi-insulating materials. The binding energy of Zn in GaN is about 0.34 eV, as determined by optical measurements.[22] A previous calculation predicted that Zn occupies Al site in AlN and the activation energy of Zn acceptor in AlN is in the range of 0.22 – 0.44 eV[23], which is

significantly smaller than that of Mg in AlN. It is thus worthy to explore Zn as an alternative *p*-type dopant in AlN. In this section, we report on the growth and PL studies of Zn-doped AlN epilayers.

Zn-doped AlN epilayers of thickness ~ 1 μm were grown by MOCVD. Prior to the growth of Zn doped layer, a 0.5 μm thick undoped AlN epilayer was first grown on sapphire substrate as a template, and was then followed by the growth of Zn-doped AlN. Dimethyl zinc (DMZn) was used as Zn source. The Zn dopant concentration was on the order of $10^{20}cm^{-3}$ as determined by SIMS measurement. The growth temperature and pressure were 1200°C and 40 torr, respectively. Hall-effect measurements were attempted to measure the conductivity of Zn-doped AlN epilayers. However, as-grown epilayers were highly resistive. Furthermore, subsequent post growth annealing of Zn-doped AlN in nitrogen ambient did not result in *p*-type conduction. Deep UV PL spectroscopy was employed to study the optical properties of Zn-doped AlN.

Low temperature (10 K) PL spectra of Zn- and Mg-doped AlN and undoped AlN epilayers are shown in Fig. 9. The PL spectrum of undoped AlN exhibits a strong band-edge emission at 6.06 eV due to the free exciton transition (FX) and virtually no impurity transitions. Since FX binding energy in AlN is around 0.08 eV, the bandgap of AlN at 10 K is thus around 6.14 eV (≈ 6.06 eV + 0.08 eV).[24] The PL spectrum of Mg doped AlN comprises a band edge transition at 6.02 eV due to the recombination of excitons bound to neutral Mg acceptors (I_1 transition). Two additional impurity emission lines at 4.70 and 5.54 eV in Mg doped AlN are also observable and believed to be donor-acceptor-pair (DAP) transitions involving two different donors (deep and shallow level donors) and Mg acceptor.[15] The deep level donors participated in the 4.70 eV transition in Mg doped AlN were identified as nitrogen vacancies with three positive charges (V_N^{3+}) that act as compensating centers for p-type doping.

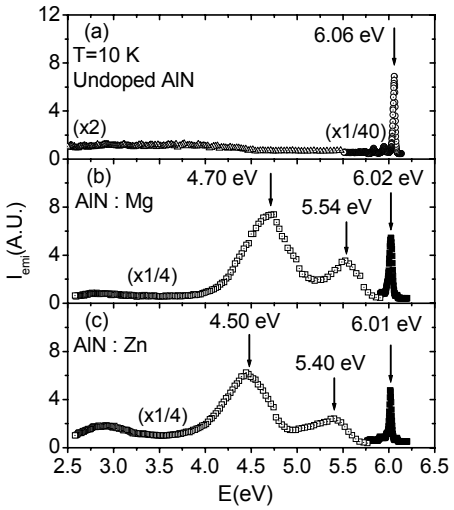

Fig. 9. PL spectra of (a) undoped, (b) Mg-doped, and (c) Zn-doped AlN epilayers measured at 10 K. For the Mg- (Zn-) doped AlN epilayers, the band edge transition at 6.06 eV disappears and a new band edge emission line is observed at 6.02 (6.01) eV. Additional impurity emission lines observed in Mg- (Zn-) doped AlN at 4.70 (4.50) and 5.54 (5.40) eV are related with Mg (Zn) acceptor impurities [After Ref.21].

Compared to the PL spectrum of Mg doped AlN, the PL spectrum of Zn-doped AlN has a very similar line shape, however, with the two impurity transitions red shifted to 4.50 and 5.40 eV (with respect to 4.70 and 5.54 eV in Mg doped AlN). The band edge emission line at 6.01 eV in Zn doped AlN can be indisputably assigned to the recombination of excitons bound to neutral Zn acceptors (I_1 transition). The measured recombination lifetime of the 4.50 eV emission line is rather long (~1 μs) and is comparable to that of the 4.70 eV line in Mg doped AlN. Based on the assignment of the 4.70 eV emission line in Mg doped AlN, we assign the emission line at 4.50 eV in Zn-doped AlN to a DAP transition of electrons bounded to nitrogen vacancies with three positive charges (V_N^{3+}) to neutral Zn acceptors, which is consistent with the measured long recombination lifetime. The width of the V_N^{3+} related emission line is very broad, which is comparable to those of the cation vacancy (V_{cation}) related emission lines in Si-doped AlN and is a typical characteristic of deep level impurity transitions. The binding energy of V_N^{3+} in AlN has been calculated to be about 0.9 eV[25], from which an energy level for Zn acceptors in AlN is thus deduced to be about 0.74 eV ($E_A \approx 6.14$ eV - 4.50 eV - 0.90 eV = 0.74 eV) with neglecting Coulomb interactions between the ionized acceptors and donors.

The temporal responses of the I_1 transition at 6.01 eV and the impurity transition at 5.40 eV in Zn-doped AlN epilayer were

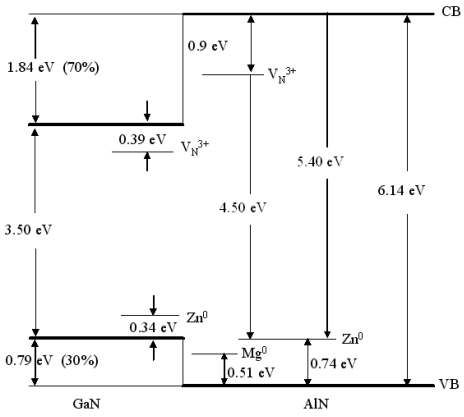

Fig. 10. Energy diagram showing the energy levels of Mg and Zn acceptors in AlN. Zn energy level in GaN is also included [After Ref. 21].

measured at 10 K, which revealed a roughly single exponential decay kinetics with a decay time constant of about 123 ps for the I_1 transition and 200 ps for the 5.40 eV impurity transition. The measured decay time constant of I_1 is comparable to a value of 130 ps observed in Mg doped AlN.[26] The recombination lifetime of 200 ps observed for the 5.40 eV emission line in Zn doped AlN is rather short, which seems to suggest that it is of a band-to-impurity type of transition. Based on this, we assign the 5.40 eV emission peak to the transition of free electrons to neutral Zn acceptors (Zn^0), although a DAP type of transition involving a shallow donor and Zn^0 cannot be totally precluded. This assignment provides an energy level of Zn acceptors in AlN to be $E_A \approx 6.14$ eV - 5.40 eV = 0.74 eV, which agrees with the value deduced from the energy position of the 4.50 eV emission line discussed above. It is worth noting that the identified origins of the two impurity transitions at 5.40 and 4.50 eV in Zn doped AlN provide an identical activation energy of 0.74 eV for Zn acceptors in AlN, which offers confidence in our assignments. Our results thus point to that the energy level of Zn is about 0.23 eV deeper than that of Mg in AlN (0.51 eV). The energy levels related to Zn acceptors and corresponding transitions in AlN are shown in Fig. 10. Optically measured Zn level in GaN is also indicated in this figure.[27]

To determine the binding energy of the Zn acceptor-bound exciton in AlN, we have measured the temperature dependence of the I_1 emission intensity in Zn doped AlN. The spectral peak position is red-shifted with increasing temperature following the variation of the bandgap. The thermal quenching of the I_1 transition is due to the dissociation of neutral acceptor-bound excitons in Zn-doped AlN. From the Arrhenius plot of the I_1 emission intensity and the least-squares fit of the data, the binding energy E_{BX} of neutral Zn acceptor bound excitons in AlN is found to be 50 meV, which is consistent with the value obtained from the difference between the spectral peak positions of FX in undoped AlN and I_1 in Zn-doped AlN epilayers (6.06 eV – 6.01 eV = 0.05 eV). Experimentally measured binding energy of neutral Mg acceptor bound excitons in AlN is about 0.04 eV. From Haynes' rule[28], the larger E_{BX} value in Zn-doped AlN compared to that in Mg-doped AlN also hints a deeper energy level of Zn than Mg in AlN.

In summary, Zn related impurity transitions were observed at 5.40 and 4.50 eV in Zn-doped AlN, which are absent on undoped AlN layers. By comparing the PL spectra of Zn-, Mg-doped and undoped AlN epilayers, the energy level of Zn acceptor in AlN was deduced to be about 0.74 eV, which is about 0.23 eV deeper than Mg level in AlN. In contrary to a previous theoretical prediction, our results thus suggest that Zn is not a better candidate than Mg as a p-type dopant in AlN.

4. SUMMARY

Of the many challenges for the development of AlGaN-based DUV photonic devices, here we addressed two fundamental issues: how to achieve *n*- and *p*-conductive AlGaN with high Al content. For Si doped *n*-AlGaN, the activation energy of Si dopant was determined with an estimated value of 190 meV for AlN. The impurity transitions in $Al_xGa_{1-x}N$ was investigated, and three distinctive groups of deep impurity transitions were observed, which were identified as $(V_{III}\text{-complex})^{2-}$ in $Al_xGa_{1-x}N$ alloys between x=0 and 1 and $(V_{III})^{3-}$ in $Al_xGa_{1-x}N$ alloys between x=0.58 and 1, and the third one $(V_{III}\text{-complex})^{1-}$ in $Al_xGa_{1-x}N$ alloys between x=0 and 1 with improved conductivity. The presence of these deep acceptor levels trap electrons, leading to the reduced conductivities of *n*-$Al_xGa_{1-x}N$. It was found that by growth optimization to reduce the cation vacancy and its complexes, the *n*-AlGaN conductivity can be significantly improved. A room temperature *n*-type resistivity as low as 0.0075 Ω·cm has been obtained for $Al_{0.7}Ga_{0.3}N$. The activation energy of Mg for *p*-type doping was also determined with a value of 0.5 eV in AlN. A strong correlation between the optical and electrical properties was observed in Mg-doped AlN, and enhanced conductivities were obtained in samples that exhibit a suppressed PL emission peak at 4.7 eV and enhanced acceptor-bound-exciton emission peak at 5.94 eV. The enhanced *p*-type conductivity is attributed to the reduced hole compensation by the donor-like intrinsic defects mainly related with V_N^{3+}. Zn-doped AlN was also studied, and the energy level of Zn acceptor in AlN was deduced to be about 0.74 eV, which is about 0.23 eV deeper than Mg level in AlN, suggesting that Zn is not a better candidate than Mg as a p-type dopant in AlN. More theoretical and experimental investigations are still required to further understand doping issues in AlGaN, particularly pertaining *p*-type doping.

ACKNOWLEDGEMENT

Our research program is supported by grants from ARO, NSF, DOE, and DARPA. This invited paper is a collection of contributions from our current and former group members: Dr. J. Li, Dr. K. B. Nam, Dr. K. H. Kim, Dr. M. L. Nakarmi, and Dr. N. Nepal.

REFERENCES

[1] V. Adivarahan, W. H. Sun, A. Chitnis, M. Shatalov, S. Wu, H. P. Maruska, and M. Asif Khan, *Appl. Phys. Lett*., **85**, 2175 (2004).
[2] Y. Taniyasu, M. Kasu, and T. Makimoto, *Nature*, **441**, 325 (2006).
[3] A. Sciuto, F. Roccaforte, S. d. Franco, and Vito Raineri, *Appl. Phys. Lett.* **89**, 0811111 (2006).
[4] C.G. Van de Walle and J. Neugebauer, *J. Appl. Phys*. **95**, 3851 (2004).
[5] T. Mattila and R.M. Nieminen, *Phys. Rev. B*. **55**, 9571 (1997).
[6] M. L. Nakarmi, K. H. Kim, K. Zhu, J. Y. Lin, and H. X. Jiang, *Appl. Phys. Lett*. **85**, 3769 (2004).
[7] Taniyasu, M. Kasu, and N. Kobayasu, *Appl. Phys. Lett*. **81**, 1255 (2002).
[8] K. B. Nam, M. L. Nakarmi, J. Y. Lin, and H. X. Jiang, *Appl. Phys. Lett*. **86**, 222108 (2005).
[9] N. Nepal, M. L. Nakarmi, J. Y. Lin, and H. X. Jiang**,** Appl. Phys. Lett. **89**, 092107 (2006).
[10] C. Stampfl and C.G. Van de Walle, *Phys. Rev.* B **65**, 155212 (2002).
[11] I. Gorczyca, N.E. Christensen and A. Svane, *Phys. Rev*. B **66**, 075210 (2002).
[12] H. S. Kim, R. A. Mair, J. Li, J. Y. Lin, and H. X. Jiang, *Appl. Phys. Lett.* **76**, 1252 (2000).
[13] D. R. Hang, C.H. Chen, Y.F. Chen, H.X. Jiang, and J.Y. Lin, *J. Appl. Phys.* **90**, 1887 (2001).
[14] T. Mattila and R. M. Nieminen, *Phys. Rev.* **B 55**, 9571 (1997).
[15] K.B. Nam, M. L. Nakarmi, J. Li, J. Y. Lin and H. X. Jiang, *Appl. Phys. Lett.* **83**, 878 (2003).
[16] J. Li, T. N. Oder, M. L. Nakarmi, J. Y. Lin, and H. X. Jiang, *Appl. Phys. Lett.* **80**, 1210 (2002).
[17] M. L. Nakarmi, N. Nepal, C. Ugolini, T. M. Altahtamouni, J. Y. Lin and H. X. Jiang, *Appl. Phys. Lett.* **89**, 152120 (2006).
[18] K.B. Nam, J. Li, M. L. Nakarmi, J. Y. Lin and H. X. Jiang, *Appl. Phys. Lett.* **82**, 1694 (2003).
[19] T. L. Tansley and R. J. Egan, *Phys. Rev*. **B 45**, 10942 (1992).
[20] N. Nepal, K. B. Nam, M. L. Nakarmi, J. Y. Lin, and H. X. Jiang, J. M. Zavada, and R.G. Wilson, *Appl. Phys. Lett*. **84**, 1090 (2004).
[21] N. Nepal, M. L. Nakarmi, H. U. Kang, J. Y. Lin, and H. X. Jiang, *Appl. Phys. Lett*., **89**, 192111 (2006).
[22] S. Nakamura and G. Fasol, The Blue Laser Diode, p. 103 (Springer, New York, 1997).
[23] F. Mireles and S. E. Ulloa, *Phys. Rev*. **B 58**, 3879 (1998).
[24] J. Li, K. B. Nam, M. L. Nakarmi, J. Y. Lin, H. X. Jiang, P. Carrier, and S. H. Wei, *Appl. Phys. Lett*. **83**, 5163 (2003).
[25] T. L. Tansley and R. J. Egan, *Phys. Rev*. **B 45**, 10942 (1992).
[26] N. Nepal, M. L. Nakarmi, K. B. Nam, J. Y. Lin, and H. X. Jiang, *Appl. Phys. Lett*. **85**, 2271 (2004).
[27] P. Bergman, G. Ying, B. Monemar, and P.O. Holtz, *J. Appl. Phys*. **61**, 4589 (1987).
[28] J. R. Haynes, *Phys. Rev. Lett*. **4**, 361 (1960).